

IHTC16-23600

# ADAPTIVE NET RADIATIVE HEAT TRANSFER AND THERMAL MANAGEMENT WITH ORIGAMI-STRUCTURED SURFACES

Brian D. Iverson\*, Rydge B. Mulford, Ernest T. Lee, Matthew R. Jones

Brigham Young University, Provo UT 84604, USA

#### **ABSTRACT**

The ability to control radiative behavior through the angular positioning of structured surfaces (e.g. the cavity effect) offers the ability to provide thermal management in dynamic radiative environments. Structures comprised of origami tessellations offer a means to achieve angular cavities that approach black-like behavior during collapse by exploiting use of the cavity effect. Expanded origami surfaces exhibit intrinsic radiative properties while collapsed surfaces exhibit increasingly black-like behavior as the cavity aspect ratio increases. Actuation of such surfaces provides the means to achieve any apparent radiative behavior between these two extremes. This work explores the use of three origami structures (finite V-groove, hinged V-groove and Miura-ori) and their respective apparent radiative properties as a function of cavity geometry using Monte Carlo ray tracing. Results are presented as a function of tessellation geometry and degree of actuation (i.e. collapse). Ray tracing models are benchmarked with V-groove geometries for which analytical models exist in the literature. Convergence for ray independence was determined to be satisfactory when the standard error of the mean for every test case was less than 0.005. Deviation in the apparent absorptivity for finite V-groove relative to the infinite V-groove is quantified. The apparent absorptivity of the Miura-ori fold exhibits sensitivity to the fold geometry when the angle of the unit cell is varied, but is relatively insensitive to the length ratio of the panel. The variable nature of the net radiative heat transfer, achievable through actuation, affords a method for thermal management of components with variable heat dissipation and/or variable radiative environments.

KEY WORDS: Radiation, Thermal Management, Origami, Variable Emissivity

# 1. INTRODUCTION

In addition to terrestrial applications, 'dynamic' control of thermal systems using radiation is critical in the thermal management of spacecraft and extraterrestrial space stations. This is primarily because, in space, radiation is the sole mode of heat exchange with the environment. Spacecraft and space exploration have significant associated costs; satellites can range from \$150 to \$800 million dollars to build [1]. Deep space and human habitat missions can have even larger associated costs. Over the life of the satellite, insurance costs total about 33% of total project costs. Between 1990 and 2006, satellite failures accounted for a loss of \$300 million per year. Approximately half of all failures were due to power related failures and 60% of all power related failures were due to three thermal management related issues including darkening of reflectors, wiring/interconnection failures and battery failures [2]. These failure modes result from heat shield degradation, thermal expansion and contraction stresses, and extreme battery operating temperatures. Radiator panels currently installed on the International Space Station deploy using rotating fluid joints between panels but remain static during operation over their lifetime [3]. Thermal management of spacecraft is a critical aspect of reliable spacecraft design.

# 1.1. Dynamic radiative properties

Control of radiative surface properties is a direct way to control thermal absorption and emission [4-7]. The ability to control the net radiative heat flux dynamically through control of radiative properties would enable thermal management of a component or surface in response to a change in the radiative environment. Intrinsic radiative surface properties are static and therefore unable to adapt to changing thermal environments. Thus,

<sup>\*</sup>Corresponding Author: bdiverson@byu.edu

for a component operating in an environment where the insolation is time varying, the static intrinsic surface properties lead to over-heating or excessive heat loss. The potential impact of adaptive control of otherwise static surface properties is precisely the argument for the proposed work [4, 6-10].

Origami-inspired surfaces, comprised of tessellations, are able to provide an adaptable surface topography to modify the apparent radiative surface behavior [11, 12]. Tessellations are the tiling of a plane with one or more repeated geometric shapes (Fig. 1a). Tessellations are the building blocks of 3D surfaces that create ordered cavities during retraction of the folds (Fig. 1b). Control of the spatial arrangement of tessellations through retraction and expansion of origami surfaces offers the ability to reconfigure surfaces and achieve variable radiative surface properties. This change in apparent properties is achieved through the cavity effect. As the tessellations that comprise the unfolded surface collapse on each other during folding, deep grooves are formed which trap radiative energy due to the high-aspect ratio of the cavity. These grooves mimic an isothermal cavity with a small opening, making the surface appear as a 'black' absorber or emitter. Controlling the cavity angle through actuation results in control of the degree of black-like behavior, making it possible for a surface to transition between the intrinsic surface property and black behavior [11, 13]. Tessellations are building blocks that enable reconfigurable surfaces with tailored apparent radiative surface properties, and controllable thermal management in a fluctuating radiative environment.

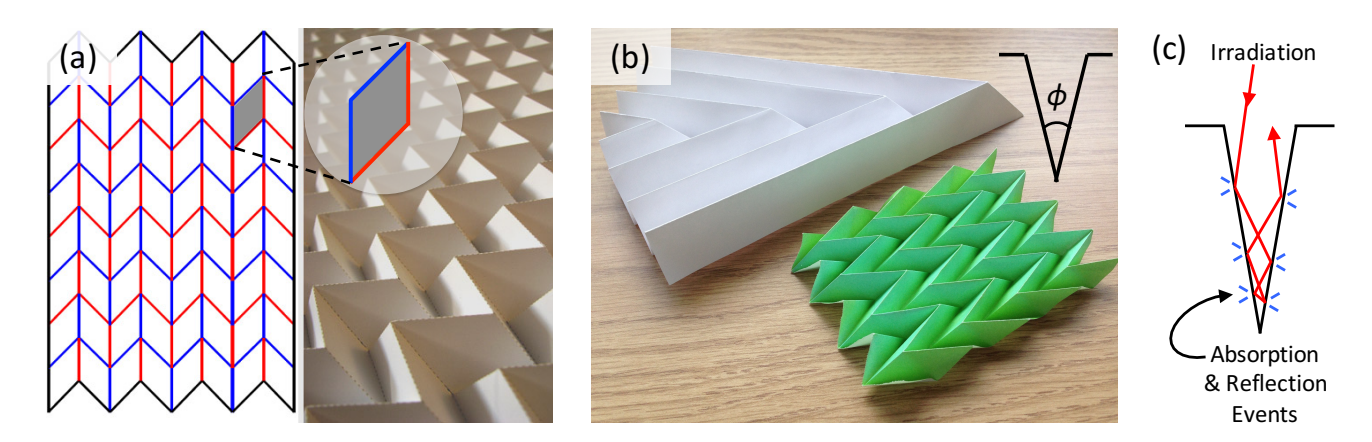


**Fig. 1.** (a) Miura-ori tessellation illustrating a 3D surface topography created by origami (adapted from [14]). (b) Examples of origami surfaces that form cavities during retraction; the inset provides V-groove dimensions. (c) Schematic of radiative reflection and absorption in high-aspect-ratio cavities that contribute to the cavity effect.

Static surfaces with grooves or cavities have been investigated in previous studies [13, 15-19]. Simple accordion folds, while effective at collapsing, have the potential to retract in one dimension and the cavities formed during retraction for accordion folds result in 2D geometries. For the V-groove surface shown in Fig. 1c, the number of possible reflections within the cavity increases as the cavity angle ( $\phi$ ) changes from a value of 180° to 0°. Multiple reflections within a cavity lead to increased apparent absorption and emission relative to a smooth surface of the same material. The increase in apparent absorption and emission for high-aspectratio cavities has been termed the cavity effect [17, 19]. Several cavity geometries have been investigated to quantify the change in radiative properties relative to a flat surface. Cylindrical, conical, spherical, rectangular and V-groove cavities are among the surface topographies that have been studied [15, 17].

Apparent absorptivity (Eq. 1) is the ratio of irradiation absorbed by a cavity ( $G_{abs}$ ) to the irradiation incident on the cavity opening ( $G_{inc}$ ) [19] and can differ from a surface's intrinsic absorptivity (absorptivity of a flat surface). Likewise, the apparent emissivity (Eq. 2) of a surface is defined by the ratio of the heat rate emitted from a cavity ( $E_{cav}$ ) divided by an equivalent blackbody surface at the cavity opening, ( $E_{cav,b}$ )

$$\alpha_a = \frac{G_{abs}}{G_{inc}} \tag{1}$$

$$\varepsilon_a = \frac{E_{cav}}{E_{cav,b}} \tag{2}$$

The apparent radiative properties are a function of intrinsic emissivity, geometry terms, actuation position, reflection mode (specular or diffuse), and, in the case of apparent absorptivity, irradiation type (collimated or diffuse). Ohwada has shown that the apparent emissivity of an isothermal cavity and apparent absorptivity of a diffusely irradiated cavity are equivalent regardless of reflection type [20].

To understand how the net radiative heat transfer of a tessellation will change with actuation we must have knowledge of the apparent radiative properties for an origami-surface. The apparent radiative properties for many conditions associated with the infinite V-groove geometry are available [19, 21, 22] but the properties for origami tessellations have not yet been developed. This work uses Monte Carlo ray tracing to explore the apparent radiative properties of three origami tessellations: finite V-groove, hinged V-groove and Miura-ori and fold pattern (Fig. 2). The impact of various parameters (including intrinsic emissivity, geometry, and reflection type) on the apparent absorptivity of the tessellation will be explored and reported. All surfaces are assumed to have diffuse emission and gray behavior in this work, with equivalent intrinsic absorptivity and emissivity.

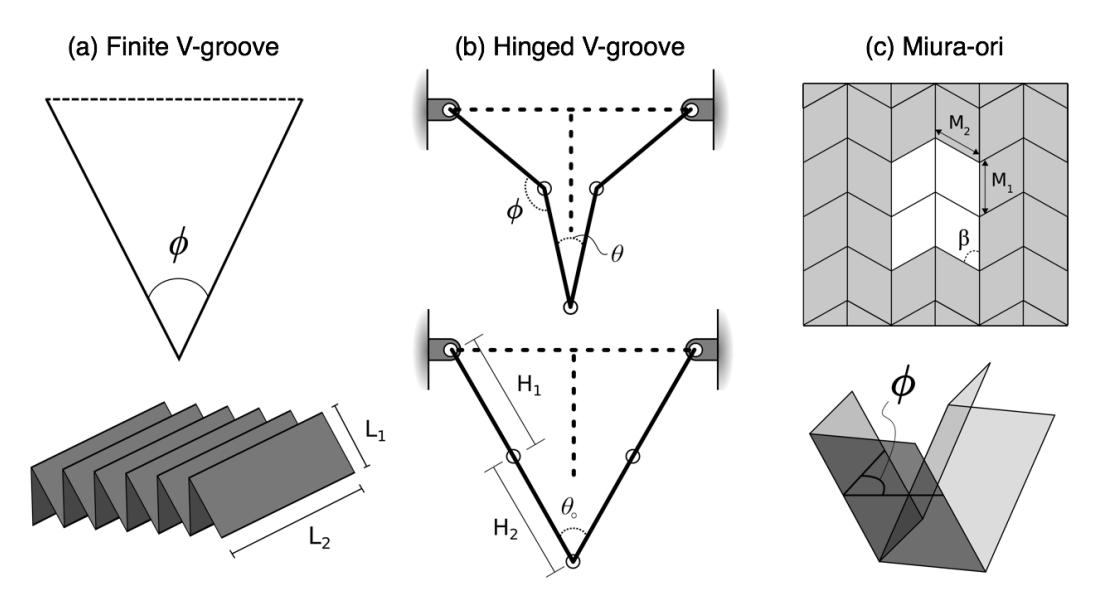


**Fig. 2.** Origami-inspired folds for surface topography manipulation. (a) finite length V-groove, (b) hinged V-groove and (c) Miura-ori (see also Fig. 1a).

# 2. TESSELLATIONS

### 2.1. Accordion

The accordion fold (Fig. 2a) consists of two flat panels, each with a width of  $L_1$  and length of  $L_2$ , with a common vertex in a "V" arrangement with angle  $\phi$ . This fold is similar to the infinite V-groove [19, 23-25] but with a finite length. The apparent radiative properties of this tessellation are a function of the surface intrinsic emissivity ( $\epsilon$ ), the ratio of panel length to panel width ( $L_2/L_1$ ) and the angle between the two panels ( $\phi$ ). The intrinsic emissivity and panel length to width ratio are inherent to the tessellation design and as such cannot be varied in real time whereas the angle between the panels may be varied through actuation of the tessellation.

The accordion fold is easy to construct making it an ideal fold for simple applications. Additionally, the finite V-groove may be found in a wide variety of applications including solar collectors, collapsible radiator panels or corrugated building materials. The apparent radiative properties of these finite V-grooves may be approximated by the available models for the infinite V-groove. However, V-grooves with a small *L/S* will not

behave the same as an infinite V-groove due to end effects. The data available in this work may be used to predict apparent radiative properties for these finite length V-grooves.

# 2.2. Hinged V-groove

Fig. 2b depicts the hinged V-groove. This surface is comprised of four panels linked end to end, with upper panels of length  $H_2$  and lower panels of length  $H_1$ . The end points on the extreme left and right edges of the joined panels are fixed at a distance of  $2H_1$ , in the same horizontal plane. The tessellation, in its most collapsed state, exhibits a "T" shape, as shown by the dotted lines in Fig. 2b, where the horizontal top of the "T" is comprised of the two panels of length  $H_1$  and the vertical portion is constructed from both panels of length  $H_2$ . During actuation, the bottom vertex is free to translate vertically, causing the "T" to open into a "V" configuration. The angle between panels of length  $H_1$  and  $H_2$  ( $\phi$ , Fig. 2b) vary from 90° to 180°. The fully extended hinged V-groove angle ( $\theta_0$ ) can vary depending on the panel length ratio,  $H_2/H_1$ . Therefore,  $\phi$  is used to track the actuation of the hinged tessellation as it always has the same angle range. For the purposes of this work, the hinged V-groove was assumed to be infinitely long in and out of the page to eliminate end effects in this initial study. The apparent radiative properties of the hinged V-groove are a function of the angle between the panels  $\phi$  (the control angle), the intrinsic radiative properties of the surfaces comprising the cavity and the ratio of panel lengths ( $H_2/H_1$ ).

When a V-groove cavity collapses, the apparent radiative properties increase with a corresponding decrease in projected surface [11]. The net effect is a decrease in net radiative heat transfer as this tessellation collapses. However, the hinged V-groove is designed to mitigate the effect of a decreasing surface area. The outer points of the hinged V-groove are pinned, causing the fold to maintain a constant projected surface area through the full range of actuation. Pinning the outer points of the hinged V-groove causes the deepest cavity possible to have a V-shape of finite depth (Fig. 2b), potentially limiting the increase in apparent radiative properties.

# 2.3. Miura-ori

A unit-cell of the Miura-ori tessellation [26] consists of four identical parallelogram-shaped panels, each with a vertical length  $M_1$  and side length  $M_2$  (see flat configuration in Fig. 2c). The angle  $\beta$  defines the angle between the two sets of parallel lines making up each panel. Two parallelograms are arranged identically and stacked vertically, forming the right half of the tessellation's unit cell. The left half is simply a reflection of the right half across the vertical axis, along the center of the unit cell. The Miura-ori tessellation is actuated by collapsing all of the parallelograms together (shown in Fig. 2c) with the angle  $\phi$  defined as the interior angle of the cavity across the reflection centerline and again tracked as the actuation angle. The apparent radiative properties of the fold are a function of intrinsic radiative properties, the ratio  $M_2/M_1$ , the angle  $\beta$  and the actuation angle  $\phi$ .

The Miura-Ori is truly a three-dimensional tessellation, where significant panel movement occurs in all three dimensions through simple linear actuation. The projected area of the Miura-ori decreases in two dimensions as the surface collapses from a flat state making it an ideal candidate for compact storage in applications where space is limited but active control of net radiative heat transfer is desired, such as an actively or passively controlled radiator on a spacecraft. Further, the cavities created by the unit-cell are 3-dimensional, likely making the surface less dependent on edge effects and finite lengths.

#### 3. METHODS

Monte Carlo ray tracing was used to determine the apparent absorptivity of the tessellated surfaces explored in this work. The in-house ray tracing program was developed in Java following the mathematical basis provided by Steinfeld [22, 27]. Cavity geometries that span the entire actuation range were modeled with the desired parameters (intrinsic emissivity, actuation angle, reflection type, etc.). An emitting surface placed at the opening of the origami cavities was used as the radiation source to determine apparent absorptivity; the number of rays emitted this surface and absorbed by the cavity were counted. The number of rays absorbed  $(N_a)$  and total number of rays emitted  $(N_t)$  can be related to apparent absorptivity [19]. Each ray is assumed to represent a unit of quantized energy [28, 29]. Each unit may be either completely reflected or completely absorbed at a single reflection event. Given this analogy, the number of absorbed rays directly indicates the rate of absorption  $(q_a)$ . With an equivalent relationship between the total number of emitted rays and the total

heat rate incident on the absorbing cavity  $(q_t)$ , the apparent absorptivity can be obtained as a function of ray tracing results, where the absorbed rays are equivalent to the escaped rays  $(N_e)$  subtracted from  $N_t$ .

$$\alpha_{a} = \frac{q_{a}}{q_{t}} = \frac{N_{a}}{N_{t}} = 1 - \frac{N_{e}}{N_{t}}$$
(3)

For diffuse emission from the source surface, random values were assigned to the polar and azimuthal angles of the emitted ray through random number generation with the polar angle weighted by a cosine distribution. With a sufficiently large quantity of rays generated, the combination of random angles approximated diffuse irradiation. The locations of intersection between a ray and a participating surface were determined with a line-plane intersection algorithm [30]. When a ray-surface interaction occurred, a new random number in the range [0,1) was compared against the absorptivity of the surface to determine if the ray was absorbed or reflected. If the ray is reflected, the new direction of the ray is determined randomly in an identical manner to that for generation of a diffuse ray from the emitting surface. For a specularly reflecting surface, the reflected ray direction was determined by rotating the ray 180° around the axis of the surface normal and then reversing the direction in which the ray is travelling. Tessellation geometries from fully extended (flat) to fully collapsed (in increments of 1°) were tested for all possible combinations of control parameters, including reflection mode (diffuse or specular), for diffuse irradiation.

#### 3.1. Validation

When performing the ray tracing analysis, a given number of rays were emitted by the source used to represent the irradiation condition for each modeled case. The standard error of the mean was then calculated for results from 20 independent ray tracing runs for each possible set of conditions at the selected ray count. If the standard error of the mean was larger than 0.005 then the test was performed again with a larger number of rays. This procedure was repeated until a ray count of 300,000 was selected, at which point the standard error of the mean fell below the established threshold for every condition. For the case of 300,000 rays, the largest standard error across all tested cases was 0.0021 and the average standard error across all tested cases was 0.00073. These values satisfied the requirement that the standard error of the mean for every case be less than 0.005.

Having acquired converged solutions, the resulting data was validated by comparing with existing solutions where available. For the finite V-groove model at the fully extended condition ( $\phi = 180^{\circ}$ ), we compared the resulting solution with the intrinsic absorptivity value, which should be recovered as a flat surface. Likewise, as the aspect ratio ( $L_2/L_1$ ) for the panels comprising a finite V-groove become large, results are expected to agree with the infinite V-groove solution. Finally, the apparent absorptivity is also expected to approach unity as the cavity angle goes to zero for specular reflection. For the hinged V-groove, it is expected that the apparent radiative properties should approach the intrinsic property values in the closed configuration ( $\phi = 90^{\circ}$ , Fig. 2a). Likewise, in the fully extended configuration ( $\phi = 180^{\circ}$ , Fig. 2a), the hinged V-groove apparent absorptivity is expected to match the apparent absorptivity for the infinite V-groove with equivalent cavity angle. Finally, for the Miura-ori, the open configuration (flat surface) should match the intrinsic absorptivity of the panels and the closed configuration is expected to approach unity for specular reflection.

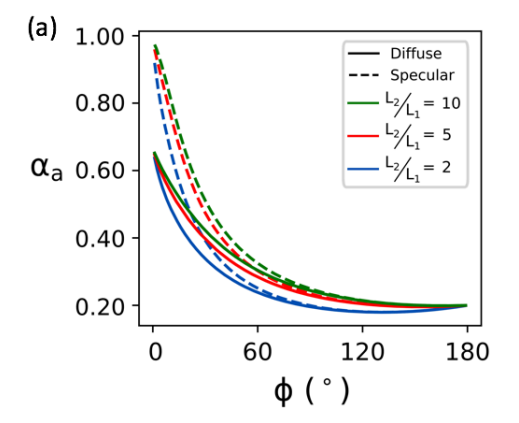
#### 4. RESULTS

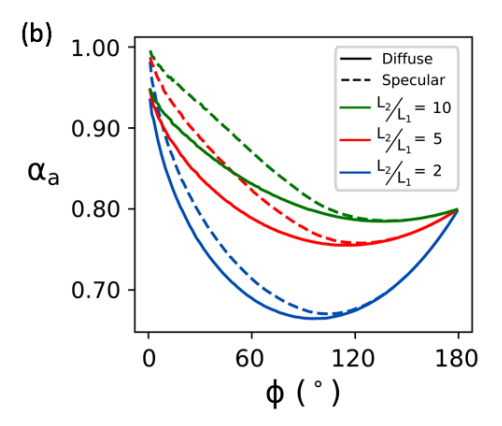
The apparent absorptivity for a diffusely irradiated, finite length V-groove is shown in Fig. 3. When considering small intrinsic absorptivity values (e.g.  $\alpha = 0.2$ , Fig. 3a), the general trend is that the apparent absorptivity increases monotonically with decreasing cavity angle, indicating greater influence of the cavity effect on absorption. This increase in apparent absorptivity with decreasing cavity angle is true for both diffuse and specular reflection at the cavity surfaces for small  $\alpha$ . However, the apparent absorptivity approaches unity for specular reflection whereas diffuse surface behavior indicates an apparent absorptivity maximum value below unity.

At high length ratios, the apparent absorptivity of the finite length V-groove approaches infinite length behavior. The highest curve of the grouping of three curves (indicated in Fig. 3 for both diffuse and specular reflection) corresponds to a length ratio of  $L_2/L_1 = 10$ . At this length ratio, the behavior of the finite V-groove approaches that of infinite V-groove behavior with an error of < 5%, for all  $\phi$  and both reflection types. Further, as  $\phi$  approaches  $180^\circ$  and flat surface geometry, the intrinsic absorptivity is recovered, as expected. Validation with flat-surface

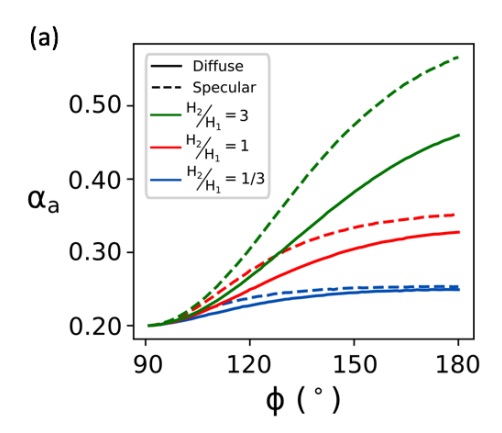
behavior and infinite V-groove behavior with increasing length ratio gives confidence in the resulting data. The apparent absorptivity value for a finite length V-groove is always lower than that for the infinite V-groove and becomes more pronounced for smaller values of  $L_2/L_1 \le 10$ .

The apparent absorptivity for a diffusely or specularly reflecting, finite length V-groove can be lower than the flat surface (intrinsic) absorptivity. This behavior becomes more pronounced for small  $L_2/L_1$  or for increasing intrinsic emissivity. Fig. 3a indicates that for  $\alpha = 0.2$  and  $L_2/L_1 = 2$ , the apparent absorptivity decreases slightly below 0.2 before rising significantly, regardless of the reflection type. For  $\alpha = 0.8$  (Fig. 3b), the apparent absorptivity decreases more significantly below the intrinsic value before increasing with decreasing cavity angle. The reason for this decrease in apparent absorptivity is a result of end effects, where additional losses are possible through the uncapped ends of the finite length V-groove. For example, a ray entering the cavity through the top cavity opening may exit the cavity through a side opening without intersecting a cavity surface.





**Fig. 3** Apparent absorptivity of a finite length V-groove for intrinsic surface emissivities of (a)  $\alpha = 0.2$  and (b)  $\alpha = 0.8$ . Sample curves are provided on each plot for a length ratio  $L_2/L_1$  of 2, 5, and 10 (see lengths, Fig. 2a). At  $L_2/L_1 \ge 10$ , the apparent absorptivity approaches that for an infinite V-groove. Solid lines represent diffuse reflection, dashed lines represent specular reflection.



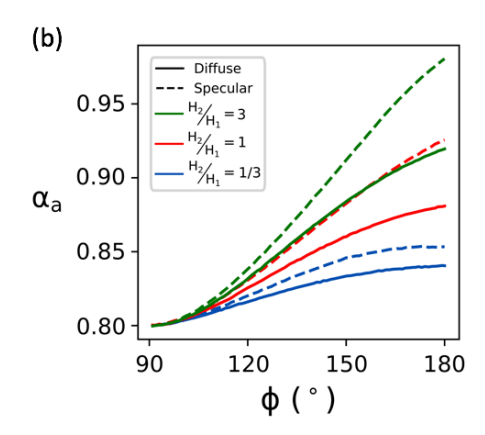


**Fig. 4** Apparent absorptivity of an infinite length, hinged V-groove for intrinsic surface emissivities of (a)  $\alpha = 0.2$  and (b)  $\alpha = 0.8$ . Sample curves are provided on each plot for a hinge length ratio  $H_2/H_1$  of 3, 1, and 1/3 (see lengths, Fig. 2b). The extended hinged V-groove angle ( $\theta_o$ ) for these length ratios is 29°, 60°, and 97°, respectively.

The apparent absorptivity behavior for a hinged V-groove is presented in Fig. 4. At  $\phi = 90^{\circ}$ , the hinged V-groove is in the "T" position and the cavity is closed and the intrinsic surface absorptivity is recovered, as expected. At  $\phi = 180^{\circ}$ , the lower vertex of the cavity is fully extended in a "V" shape with apparent absorptivity values that correspond with that obtained for an infinite V-groove  $(L_2/L_1 \sim 10)$  for specular or diffuse reflection. Generally, the apparent absorptivity increases with increasing hinge length ratio  $H_2/H_1$ , as this results in a

smaller nominal angle in the fully extended position,  $\theta_o$ , and increases the apparent absorptivity range by increasing the possible extent of the cavity effect.

The effect of the intrinsic surface property can be observed by comparing Fig. 4a with Fig. 4b. As the intrinsic surface absorptivity increases, the possible range of apparent absorptivity decreases. For example, the apparent absorptivity for a specularly reflecting, hinged V-groove cavity of  $H_2/H_1 = 3$  varies roughly from 0.2 to above 0.5 with increasing  $\phi$  (Fig. 4a). However, the upper limit of the apparent absorptivity can approach unity with increasing hinge length ratio  $H_2/H_1$ , resulting in a possible change in apparent absorptivity from 0.2 to 1. Since the minimum apparent absorptivity for the hinged V-groove is equivalent to the intrinsic absorptivity, the possible range of apparent absorptivity values is compressed for higher intrinsic absorptivity values. For example,  $\alpha_a$  varies from 0.8 to a maximum of 1 (Fig. 4b) when the intrinsic surface absorptivity is 0.8, regardless of hinge length ratio  $H_2/H_1$ . As noted previously, the hinged V-groove offers the possibility for a fixed projected area while also bounding the lower limit of the apparent surface behavior by the intrinsic properties.

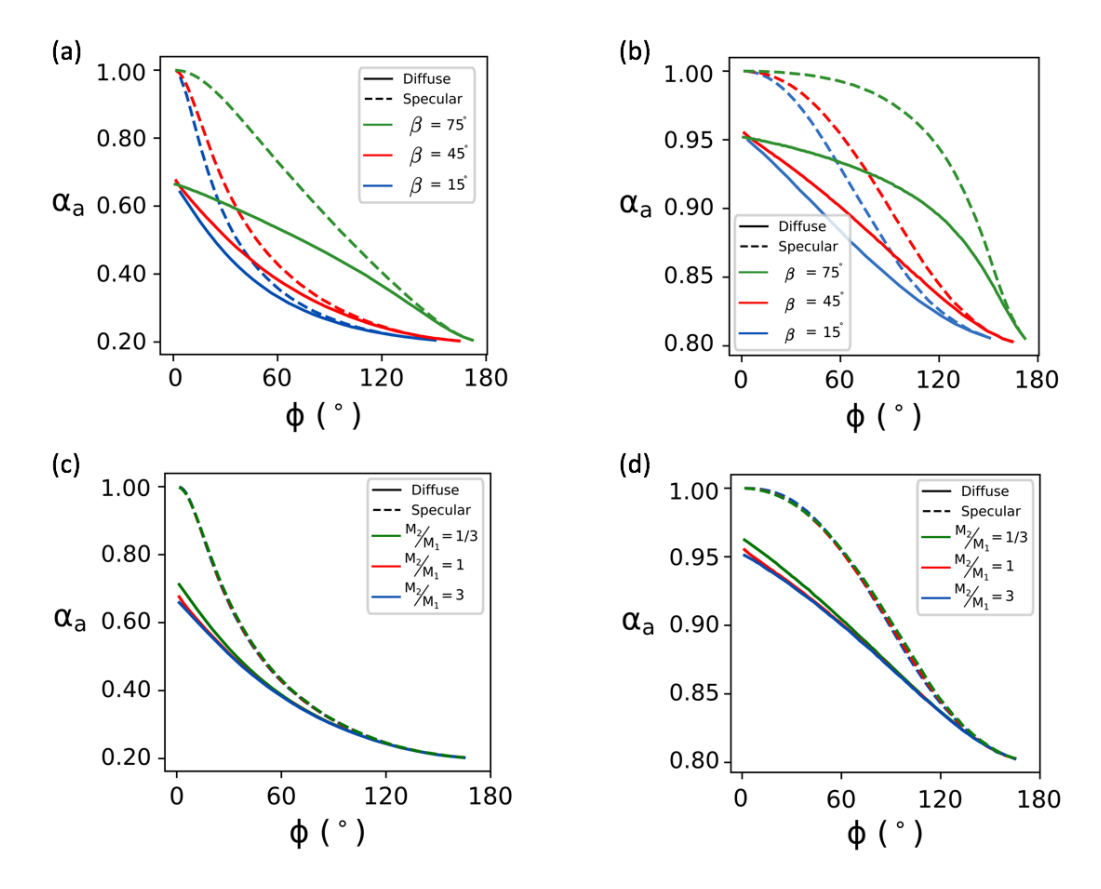


**Fig. 5** Apparent absorptivity of a Miura-ori surface of length ratio  $M_2/M_1 = 1$  and intrinsic absorptivity (a)  $\alpha = 0.2$  and (b)  $\alpha = 0.8$ . Sample curves are provided on each plot for  $\beta$  angles of 15°, 45° and 75° (see geometry, Fig. 2c). Apparent absorptivity at a fixed  $\beta = 45^\circ$  and intrinsic absorptivity (c)  $\alpha = 0.2$  and (d)  $\alpha = 0.8$  are also provided with sample curves of varying length ratio  $M_2/M_1$  of 1/3, 1, and 3.

Fig. 5 provides the apparent absorptivity behavior with respect to actuation angle for the Miura-ori tessellation. As in all previous cases, specular reflection causes a cavity to approach black behavior as the actuation angle collapses towards zero. Diffuse reflection achieves an apparent absorptivity value lower than unity but larger than the intrinsic absorptivity of the material when the cavity is fully collapsed. Fig. 5a and Fig. 5b ( $\alpha = 0.2$  or  $\alpha = 0.8$ , respectively) depict the variation of apparent absorptivity with respect to  $\phi$  for  $M_2/M_1 = 1$  and  $\beta$  values of 15°, 45°, and 75°. For either specular or diffuse reflection, the apparent absorptivity increases with  $\beta$  for equivalent values of  $\phi$ , where a value of  $\beta = 75^{\circ}$  shows a significant increase in apparent absorptivity as compared to smaller  $\beta$  values. A large  $\beta$  value corresponds to a unit cell that is comprised of panels that are increasingly more like squares than parallelograms. The more 'square' the panels become, the more rapidly

the cavities begin to exhibit a vertical depth, leading to an early increase in apparent absorptivity of the unit cell for relatively large  $\phi$  values.

Fig. 5c and Fig. 5d ( $\alpha = 0.2$  or  $\alpha = 0.8$ , respectively) exhibit apparent absorptivity behavior with respect to actuation angle  $\phi$ , where  $\beta$  is held constant at a value of 45° and  $M_2/M_1$  is assigned values of 1/3, 1 or 3. For specular reflection, the ratio  $M_2/M_1$  exhibits a negligible influence on apparent absorptivity regardless of intrinsic absorptivity; similar behavior is seen for all values of  $\beta$  tested (15°, 45°, 75°). In the case of diffuse reflection, a slight change of apparent absorptivity is seen with  $M_2/M_1$  for  $\phi < 30^\circ$ , although the variation is small when compared to the impact of  $\beta$  on apparent absorptivity. As the intrinsic absorptivity increases, the deviation in apparent absorptivity with  $M_2/M_1$  decreases, noting the difference in scales between Fig. 5c and d. Overall, the length ratio  $M_2/M_1$  does not play a significant role in the cavity effect for the Miura-ori tessellation. This is because a unit cell of the Miura-ori tessellation contains multiple finite-length V-groove cavities, with some arranged vertically and some arranged horizontally (see Fig. 2c). Increasing the ratio  $M_2/M_1$  below or above unity increases the length of one intrinsic V-groove while decreasing the length of the opposing intrinsic V-groove. Despite these variations in length, the total length of the resulting V-groove cavities remains approximately the same.

#### 5. CONCLUSIONS

The apparent absorptivity for a finite length V-groove, hinged V-groove and Miura-ori surface irradiated diffusely has been determined as a function of the actuation angle, fold geometry and diffuse or specular reflection. Solutions are provided for cavities comprised of isothermal, gray surfaces with diffuse emission. The apparent emissivity of an isothermal cavity that is diffusely irradiated is equivalent to the apparent absorptivity, regardless of reflection type [20]. The above apparent radiative properties may be useful in determining the net radiative heat transfer for surfaces that collapse and could be used in predicting the thermal performance of a variable radiator comprised of these fold types.

Results indicate that a finite length V-groove can be approximated with an infinite V-groove model with an error of less than 5% when  $L_2/L_1 \le 10$ . An apparent absorptivity less than the intrinsic surface absorptivity is possible for the finite V-groove and becomes more pronounced for large intrinsic absorptivity and small length ratios,  $L_2/L_1$ . We demonstrate the range of possible apparent absorptivity values for the hinged V-groove can be limited relative to the V-groove, but offers the potential for a fixed projected area. However, the length ratio  $H_2/H_1$  increases the possible range of apparent absorptivity making it possible to approach V-groove behavior. The apparent absorptivity for the Miura-ori tessellation is affected predominantly by the  $\beta$  angle and not by the length ratio  $M_2/M_1$ .

# **ACKNOWLEDGMENT**

This work is funded by a NASA Space Technology Research Fellowship, grant number NNX15AP49H and Brigham Young University.

# **NOMENCLATURE**

$E_{cav}$	Cavity emissive power (W/m <sup>2</sup> )	$N_e$	Number of escaped rays (-)
$E_{cav,b}$	Blackbody emissive power	$N_t$	Total number of emitted rays (-)
	at cavity opening (W/m <sup>2</sup> )	$q_a$	Absorbed heat rate (W)
$G_{abs}$	Absorbed irradiation (W/m <sup>2</sup> )	$q_t$	Total incident heat rate (W)
$G_{inc}$	Incident irradiation (W/m <sup>2</sup> )	$\dot{\alpha}$	Intrinsic absorptivity ( - )
$L_1$	V-groove panel width (m)	$\alpha_a$	Apparent absorptivity ( - )
$L_2$	V-groove panel length (m)	β	Parallelogram angle (Miura) (°)
$H_1$	Upper hinged panel length (m)	$\varepsilon$	Intrinsic emissivity ( - )
$H_2$	Lower hinged panel length (m)	$\mathcal{E}_a$	Apparent emissivity ( - )
$M_1$	Tesselation vertical length - Miura (m)	$\phi$	Control angle (°)
$M_2$	Tesselation side length - Miura (m)	$\dot{ heta_0}$	Fully extended hinged angle (°)
$N_{a}$	Number of absorbed rays (-)		

# REFERENCES

- [1] Saleh, J. H. and Castet, J. F., 2011, Spacecraft Reliability and Multi-State Failures. West Sussex, U. K., John Wiley & Sons.
- [2] Landis, G. A., Bailey, S. G., and Tischler, R., 2006, "Causes of power related satellite failures," 4th World Conference on Photovoltaic Energy Conversion.
- [3] NASA, "International Space Station," accessed October 15, 2016 from <a href="http://spaceflight.nasa.gov/gallery/images/shuttle/sts-135/hires/iss028e016140.jpg">http://spaceflight.nasa.gov/gallery/images/shuttle/sts-135/hires/iss028e016140.jpg</a>.
- [4] Hill, S. A., Kostyk, C., Motil, B., Notardonato, W., Rickman, S., and Swanson, T., 2012, "Thermal Management Systems Roadmap, Techology Area 14," April 2012, NASA.
- [5] Hengeveld, D. W., Mathison, M. M., Braun, J. E., Groll, E. A., and Williams, A. D., 2010, "Review of modern spacecraft thermal control technologies," *HVAC&R Research*, Vol. 16, pp. 189-220.
- [6] Shannon, K. C., Sheets, J., Groger, H., Storm, R., and Williams, A., 2008, "Thermal management integration using plug and play variable emissivity devices," 22<sup>nd</sup> Annual AIAA/USU Conference on Small Satellites, August 11-14, 2008, Logan, UT.
- [7] Grob, L. M. and Swanson, T. D., 2000, "Parametric study of variable emissivity radiator surfaces," AIP Conference Proceedings, Vol. 504, pp. 809.
- [8] Biter, W., Hess, S., Oh, S., Douglas, D., and Swanson, T., 2005, "Electrostatic radiator for satellite temperature control," IEEE Aerospace Conference, March 5-12, 2005, Big Sky, MT.
- [9] Demiryont, H., Shannon, K. I., and Ponnappan, R., 2006, "Electrochromic Devices for Satellite Thermal Control," Space Technology and Applications International Forum.
- [10] Swanson, T., Motil, B., Chandler, F., Bruce, W., Dinsmore, C., Kostyk, C., Lysek, M., Rickman, S., and Stephan, R., 2015, "NASA Technology Roadmaps, TA 14: Thermal Management Systems," May 2015 Draft, NASA.
- [11] Mulford, R. B., Jones, M. R., and Iverson, B. D., 2016, "Dynamic control of radiative surface properties with origami-inspired design," *Journal of Heat Transfer*, Vol. 138, pp. 032701.
- [12] Blanc, M. J., Mulford, R. B., Jones, M. R., and Iverson, B. D., 2016, "Infrared visualization of the cavity effect using origami-inspired surfaces," *Journal of Heat Transfer*, Vol. 138, pp. 020901.
- [13] Mulford, R. B., Jones, M. R., and Iverson, B. D., 2015, "Net radiative heat exchange of an origami-inspired, variable emissivity surface," ASTFE Thermal and Fluids Engineering Summer Conference, August 9-12, 2015, New York, NY.
- [14] Itai Cohen Group, "Miura-ori by Koryo Miura," accessed November 22, 2017 from https://cohengroup.lassp.cornell.edu/research/origami.
- [15] Modest, M. F., 2013, Radiative Heat Transfer, 3rd ed. New York, Academic Press.
- [16] Howell, J. R., Siegel, R., and Menguc, M. P., 2011, Thermal Radiation Heat Transfer. Boca Raton, FL, CRC Press.
- [17] Sparrow, E. M. and Cess, R. D., 1978, Radiation Heat Transfer. New York, McGraw-Hill.
- [18] Hollands, K. G. T., 1963, "Directional selectivity, emittance, and absorptance properties of vee corrugated specular surfaces," *Solar Energy*, Vol. 7, pp. 108-116.
- [19] Sparrow, E. M. and Lin, S. H., 1962, "Absorption of thermal radiation in a V-groove cavity," *International Journal of Heat and Mass Transfer*, Vol. 5, pp. 1111-1115.
- [20] Ohwada, Y., 1988, "Mathematical proof of an extended kirchhoff law for a cavity having direction-dependent characteristics," *Journal of the Optical Society of America a-Optics Image Science and Vision*, Vol. 5, pp. 141-145.
- [21] Sparrow, E. M. and Lin, S. L., 1965, "Radiation heat transfer at a surface having both specular and diffuse reflectance components," *International Journal of Heat and Mass Transfer*, Vol. 8, pp. 769-779.
- [22] Mulford, R. B., Collins, N. S., Farnsworth, M. S., Jones, M. R., and Iverson, B. D., 2018, "Total hemispherical apparent radiative properties of the infinite V-groove with specular reflection," *International Journal of Heat and Mass Transfer*, Vol. 124, pp. 168-176.
- [23] Daws, L. F., 1954, "The emissivity of a groove," British Journal of Applied Physics, Vol. 5, pp. 182 187.
- [24] Zipin, R. B., 1966, "The apparent thermal radiation properties of an isothermal v-groove with specularly reflecting walls," *Journal of Research of the National Bureau of Standards*, Vol. 70c, pp. 275-280.
- [25] Zipin, R. B., 1965, *The directional spectral reflectance of well characterized symmetric v grooved surfaces*, Doctorate Thesis, Purdue University, Ann Arbor, Michigan.
- [26] Miura, K., 1985, "Method of packaging and deployment of large membrances in space," *The Institute of Space and Astronautical Science*, Vol. 618, pp. 1-9.
- [27] Steinfeld, A., 1990, "Apparent absorptance for diffusely and specularly reflecting spherical cavities," *International Journal of Heat and Mass Transfer*, Vol. 34, pp. 1895-1897.
- [28] Baumeister, J. F., 1990, "Thermal radiation characteristics of nonisothermal cylindrical enclosures using a numerical ray tracing technique," 5th Thermophysics and Heat Transfer Conference, Seattle, Washington.
- [29] Baumeister, J. F., 1993, "Application of ray tracing in radiation heat transfer," *Thermal and Fluids Analysis Workshop*, Cleveland, Ohio, pp. 1-53.
- [30] Foley, J., van Dam, A., Feiner, S., and Hughes, J., "Clipping lines," in *Computer Graphics*, 3rd ed: Addison-Wesley Proffesional, 2013.